European Journal of Radiology 112 (2019) 153–160

Contents lists available at ScienceDirect

European Journal of Radiology

journal homepage: www.elsevier.com/locate/ejrad

Research article

Development of an anthropomorphic spine phantom suitable for fusion of MR neurography with interventional flat-panel CT

Adrian Kobe[a], Matthias Zadory[b], Qeumars M. Hamie[a], Johannes M. Froehlich[c], Markus Klarhöfer[d], Thilo Elsässer[d], Thomas Pfammatter[a], Roman Guggenberger[a,*]

[a] Institute of Diagnostic and Interventional Radiology, University Hospital Zurich, Zurich, Switzerland
[b] KlusLab Research, Zurich, Switzerland
[c] Guerbet AG, Zurich, Switzerland
[d] Siemens Healthcare AG, Zurich, Switzerland

ARTICLE INFO

Keywords:
Anthropomorphic spine phantom
Image fusion
Magnetic resonance neurography
Spine interventions

ABSTRACT

Purpose: To design a spine phantom suitable for fusion of MR neurography (MRN) with interventional flat panel computed tomography (FPCT) images from tissue-equivalent agarose gels and artificial nerves in MRI, including material with equal attenuation to bone in computed tomography (CT).

Methods: T1-/T2-relaxation times of target tissue were determined in vivo (n = 5) using MR mapping-techniques. Serial dilution of castor oil lipogels was performed ex vivo in order to define correct composition for tissue-equivalent relaxation times. Similarly, serial dilution series of calcium carbonate ($CaCO_3$) and barium sulphate ($BaSO_4$) in synthetic resin were used to adjust radiodensity of selected vertebral bodies (L1-L5) and sacrum in CT. Nerve tissue was simulated with agarose-impregnated polyethylene fibers. Spine phantom was assembled using respective components in anthropomorphic geometry. A fat-saturated, T2-weighted 3D SPACE STIR sequence was acquired for MRN and subsequently fused with an on-site FPCT scan of the phantom.

Results: In vivo T1-/T2-values for fat tissue were found to be at 394 ± 16 ms and 161 ± 16 ms, corresponding to a castor oil concentration of 50%. Analogously, bone marrow-equivalent values were measured at 822 ± 21 ms and 67 ± 6 ms, simulated with 40% castor oil. Cortical bone-like radiodensity of 1'115 ± 80 HU was achieved for artificial bone with 30% $CaCO_3$ and 1.5% $BaSO_4$. Simulated nerves were successfully depicted in MRN and fused with FPCT, combining optimal contrasts for nerves and bones on-site.

Conclusions: The customized phantom showed analogous tissue contrasts to in vivo conditions in both MRN and FPCT, facilitating simulations of fusion-image guided spine interventions.

1. Introduction

Anthropomorphic phantom models are useful for the development and implementation of new interventional procedures due to long-term structural stability without concern for radiation dose, patient motion or discomfort [1,2]. Recent advances in interventional radiology are aiming to combine different imaging modalities, e.g. ultrasound, magnetic resonance imaging (MRI) and computed tomography (CT) in hybrid fashion in order to take advantage of the complementary strengths and contrasts [3–5].

Indeed, intraprocedural quick on site image fusion has gained increasing interest in recent years. With recent flat panel computed tomography (FPCT) technology, intraprocedural fluoroscopy and cone-beam CT scan can be acquired within the same session, serving as road maps for ensuring trajectory planning for needle-guided interventions. Spinal interventions usually rely on fluoroscopy or CT in order to help define high contrast structures, e.g. bony landmarks for perineural medical interventions (e.g. injection, lumbal punction), kypho-/vertebroplasty or local ablative procedures [6,7]. However, soft tissues and especially nerve structures cannot be depicted in FPCT due to its low contrast resolution.

Recent advances in MR technology have sparked interest in optimal nerve depiction using dedicated magnetic resonance neurography (MRN) sequences [8,9], including information on functional nerve

Abbreviations: $BaSO_4$, barium sulphate; $CaCO_3$, calcium carbonate; CT, computed tomography; FOV, field of view; FPCT, flat panel computed tomography; HU, hounsfield unit; MIP, maximum intensity projections; MRI, magnetic resonance imaging; MRN, magnetic resonance neurography; ROI, region of interest; SPACE, Sampling Perfection with Application optimized Contrasts using different flip angle Evolution; STIR, Short Tau Inversion Recovery; TE, echo time; TR, repetition time

* Corresponding author at: Institute of Diagnostic and Interventional Radiology, University Hospital Zurich, Rämistrasse 100, 8091 Zurich, Switzerland.
E-mail address: roman.guggenberger@usz.ch (R. Guggenberger).

https://doi.org/10.1016/j.ejrad.2019.01.019
Received 12 November 2018; Received in revised form 12 January 2019; Accepted 20 January 2019

status by diffusion weighted-imaging [10]. T2-weighted, fat-saturated images at high resolution allow depicting nerves as high contrast structures with respect to surrounding tissues with large field of views. Modern radiofrequency-coils and scanners operating at high field strength (e.g. 3.0 T) increase signal-to-noise ratio of target volumes and structures. Ensuing post-processing possibilities, e.g. maximum intensity projections (MIP) of 3D data can then nicely illustrate complex anatomic regions, e.g. brachial or lumbosacral plexus and highlight pathology [11].

Following anatomic landmarks, combining MRN with FPCT or fluoroscopy helps to depict and fuse different tissue compartments at the same time, such as X-ray attenuating bone material in combination with nerve structures associated with high signal on T2-weighted MR sequences. This helps the treating physician to plan and perform the intervention more accurately with respect to nerve tissue.

There has been intensive research in creating adequate solid materials for MRI or CT phantoms, among them agarose, agar, polyvinyl alcohol, gelatin and polyacrylamide interblended with paramagnetic ions (e.g. $GdCl_3$) to control the relaxation times [12,13]. However, a spine phantom that allows for sufficient tissue simulation of bone, soft tissue and nerve structures in both, MRI and CT at the same time is still lacking.

Purpose of this study was to design a spine phantom suitable for fusion of MR neurography with interventional flat panel computed tomography images from tissue-equivalent agarose gels and artificial nerves in MRI, including material with equal attenuation to bone in computed tomography.

2. Material and methods

Local institutional review board approval was obtained for all MRI examinations and written informed consent was obtained from each volunteer. Retrospective attenuation measurements on spine CTs in our image database were approved by the local institutional review board waiving informed consent. To develop the present anthropomorphic phantom, we followed the manufacturing process as depicted in the flow chart in Fig. 1. First in vivo and ex vivo MR and CT analyses were performed yielding all required parameters needed for the creation of the anthropomorphic phantom. Ultimately MRN of the phantom was performed and fused with FPCT.

2.1. In vivo MR and CT study

Five healthy volunteers (three women; mean age 28.4 ± 1.9 years) with neither history nor physical findings of current disease or known contraindications to MR (e.g. pregnancy, metallic implants) were enrolled in the study and underwent MRI of the lumbar spine at 3.0 T (Siemens MAGNETOM Skyra, Siemens Healthineers, Erlangen, Germany) with an 18-channel body coil and a 32-channel spine array (Siemens Healthineers, Erlangen, Germany). T1 and T2 maps at axial L3-L4 level containing adequate portion of muscle, subcutaneous fat and bone marrow were obtained. A variable flip angle technique was used for T1 mapping and a multi-echo spin-echo sequence for T2 mapping (Fig. 2). For 2D T1 mapping the following standard gradient-recalled-echo MR scan parameters were used: repetition time (TR) 3 ms, echo time (TE) 1.32 ms, flip angle 8° and 15°, slice thickness 8 mm, field of view (FOV) 380 mm^2. For T2 mapping: TR 2500 ms, eight echo times from 10 ms to 80 ms, flip angle 90°, slice thickness 8 mm, FOV 380 mm^2. After adequate instruction, regions of interest (ROI) were placed by hand in the selected portion of tissue by a junior fellow in order to measure relaxation times and their mean values. In each subject, three measurements per tissue type were used to determine average T1 and T2 relaxation times. These values were used as reference for the ensuing ex vivo phantom fabrication and validation.

Similar to MR measurements, Hounsfield unit values in CT images were measured on axial images of lumbar spine MDCT scans in 5 retrospectively selected healthy patients (mean age 28.2 ± 2 years) of our local image database. ROIs were placed in the cortical bone (2 mm diameter) of the vertebral pedicle and inside the vertebral body of the vertebrae L2-L5 (2 cm diameter) in order to obtain bone cortex and marrow density. Any diseases affecting bone health, e.g. dietary or endocrinologic problems, traumatic, degenerative or congenital conditions were excluded in advance. For all patients the same CT scanner and scan protocol had been used (SOMATOM® Definition Flash, Siemens Healthineers, Erlangen, Germany; tube voltage 120 kV, mean tube current 229 ± 9.2 mAs, mean CTDIvol 15.1 ± 1 mGy). Axial

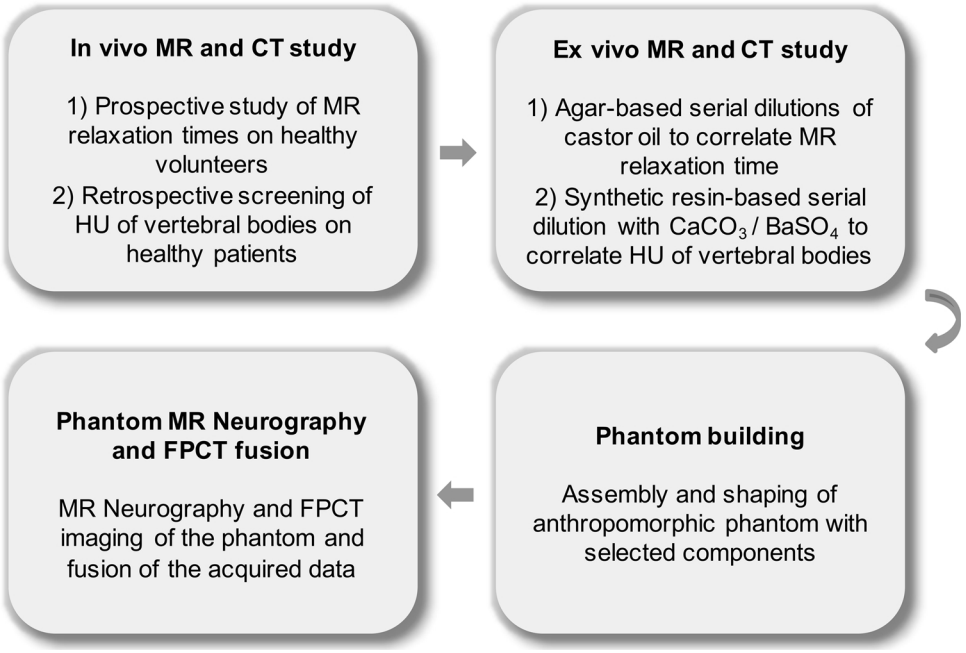

Fig. 1. Flow-chart illustrates fabrication of spine phantom for image fusion of MRN with FPCT. In a first step, in vivo measurements in MR were performed in order to determine physiological MR relaxation times of muscle, fat and bone marrow tissue. Attenuation of vertebral bones in CT was measured on PACS-archived prior CT studies of the lumbar spine in healthy patients.
Based on in vivo tests, ex vivo simulation of different tissues was performed using agar-based serial dilutions of castor oil for adjusting MR relaxation times and synthetic resin-based serial dilutions with barium-sulfate ($BaSO_4$) for adjusting vertebral bone attenuation.
Using corresponding relaxation times and attenuation characteristics, the anthropomorphic spine phantom was designed and assembled.
In a last step, FPCT and MRN of the spine phantom were acquired and could be successfully fused on a single image.

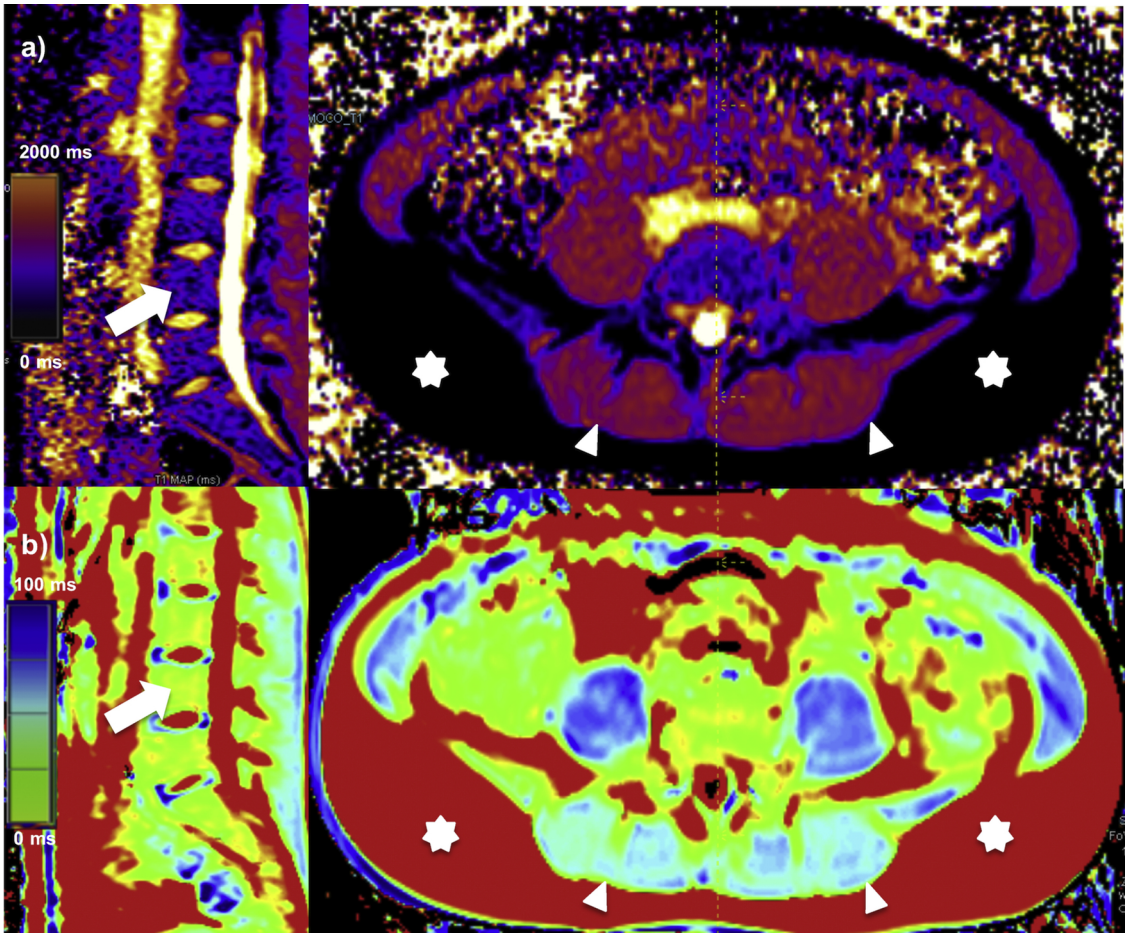

Fig. 2. In vivo images acquired at 3.0 T: T1 and T2 relaxation time maps of a healthy volunteer. T1 (a) and T2 (b) relaxation times were measured in fat tissue (star; axial image), muscle (arrowhead; axial image) and bone marrow (arrow; sagittal image).

images were reconstructed with 2 mm slice thickness and with 2 mm increment using a reconstruction field of view of 20 cm and a standard high convolution bone-kernel (I50f).

2.2. Experimental set-up for the ex vivo MR and CT study

Due to its relative high hydrophilicity, castor oil (Hänseler AG, Herisau, Switzerland) was used as relaxation-modifying agent in order to cover a large range of different relaxation times. The phantom was composed of the following components: 1.5% agarose as jellifying agent, purified water (added to the desired amount of gels), 0.5% Polyoxyethylen (20)-sorbitan-monooleate (polysorbate 80, Hänseler AG, Herisau, Switzerland) as emulsifier and castor oil. In order to simulate T1 and T2 times of the different tissues the proportion (%) of castor oil was varied. For instance 100 g of lipogel with 40% castor oil consisted of 1.5 g agarose, 0.5 g polysorbate, 40 g castor oil and 58 g water.

The agarose was sprinkled into purified water at 80 °C and heated for 5–10 minutes until fully dissolved. The preheated 80 °C warm castor oil mixed with the emulsifier was added to the agarose solution. The resulting mixture was stirred while being kept at 80 °C ensuring homogeneity of the resulting lipogel. The castor-oil agarose lipogel was then poured into falcon tubes embedded into agarose gel for further MR T1 and T2 mapping acquisitions (Fig. 3a and b) using equal imaging parameters to in vivo measurements. A series of lipogels with castor oil concentrations varying from 0 to 100% were prepared in order to determine the ideal concentration of castor oil for human tissue MR simulation of fat, muscle and bone marrow.

Likewise, serial dilutions of calcium carbonate ($CaCO_3$) and barium sulphate ($BaSO_4$) (Sigma-Aldrich, Merck, Buchs, Switzerland) in synthetic polyurethane resin were used to adjust mean radio density to selected vertebral bodies (L2-L5) from patient CT scans of the lumbar spine (Fig. 3c). The polyurethane resin is a liquid composed of two parts (Part A and B). Once these two components are mixed (1:1 by weight) together with the $CaCO_3$ (dry chemical) and $BaSO_4$ (liquid) the mixture will cure.

In order to simulate nerve tissues and generate clear visibility on the SPACE STIR MRN “workhorse” sequence, multiple rolled polyethylene fibers impregnated with a 2% agarose gel and dried overnight were used.

2.3. Phantom building

Based on the results of the in vivo MR and CT study, we used the appropriate concentration of castor oil / $CaCO_3$ and $BaSO_4$ for each simulated tissue (fat, muscle, bone marrow), imitating appropriate tissue attenuation and relaxation characteristics in CT and MR. Thus various simulated tissue-equivalent lipogels were used as a basis for the subsequent forming of various anthropomorphic structures of the lumbar spine region. For simulation of the iliopsoas and erector spinae muscles, the lipogel were poured into a thin polypropylene membrane in order to create the appropriate muscle forms. A Sawbones® lumbar spine and sacrum model (Sawbones, Vashon Island, WA) were used as a positive frame. Using silicone, a negative imprint of this model was obtained. Subsequently the negative imprint was casted with the adequate mixture of synthetic resin (68.5% of the mixture), $CaCO_3$ (10%)

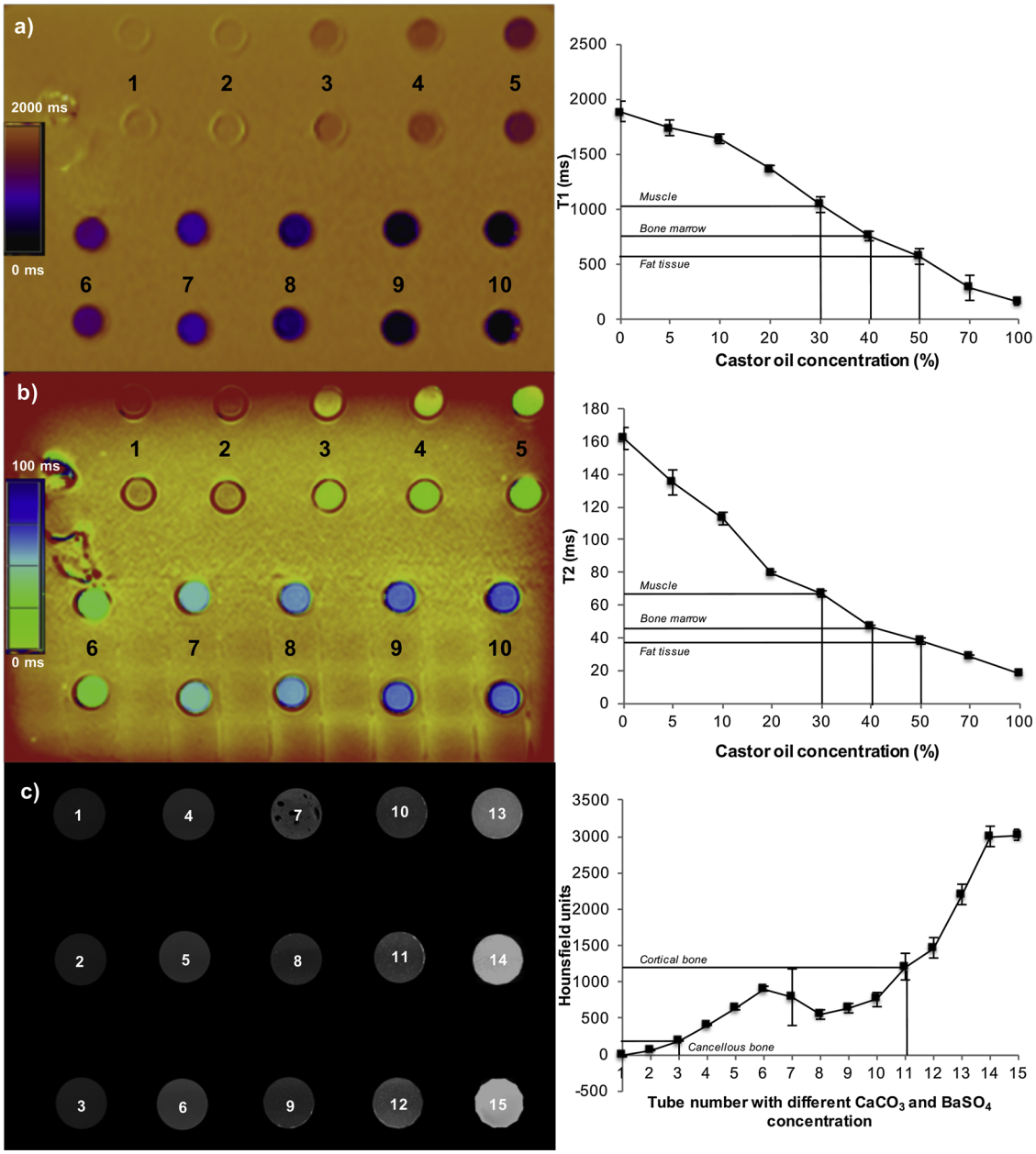

Fig. 3. Ex vivo relaxation time mappings of castor oil serial dilutions and ex vivo Hounsfield unit measurements.
a) and b) show T1 and T2 relaxation time mappings, respectively in an ex-vivo model of paired vials of each mixture composed of agarose, purified water, Polyoxyethylen (20)-sorbitan-monooleate and varying castor oil concentrations (as demonstrated on the x-axis on the right). Figure c) illustrates the attenuation measurements (HU) of a composition of polyurethane resin with varying $CaCO_3$ and $BaSO_4$ concentrations (the different tube concentrations can be found in Tables 1 and 2).

and $BaSO_4$ (1.5%) to imitate cortical bone. This initially heated mixture, imitating cortical bone, was chilled to room temperature under constant rotation until solidified in the desired anatomic shape. Constant rotation was achieved manually by rotating the mould in all three-dimensions at a rate of approximately 20 rotations per minute for about 4 min until solidification. The constant rotation resulted in cavities in the vertebral bodies. These were filled with a lipogel, imitating bone marrow relaxation time characteristics. The filaments for the nerve fibers were fixed in the spinal canal exiting through respective neuroforamen in order to match as close as possible nerve course and anatomy. Intervertebral discs were generated by polyethylene foam pads fixed with 2% agarose gel. The entire assembly consisting of artificial bone, discs, muscles and nerves was then embedded in lipogel imitating visceral und subcutaneous fat tissue, resulting in a cylindric shaped anthropomorphic spine phantom measuring 22 × 14 × 8 cm (Fig. 4).

2.4. Phantom MR neurography and FPCT fusion

All MR acquisitions were performed on the same 3.0 T unit (MAGNETOM Skyra, Siemens Healthineers, Erlangen, Germany) using an 18-channel body coil as described above. Prior to T1 and T2 relaxation time mapping, anatomical imaging of the anthropomorphic phantom was performed in axial and sagittal position using standard T2-weighted sequences (TR 2020 ms, TE 95 ms, turbo factor 31, refocusing angle 130°, slice thickness 3 mm, FOV 260 mm^2) and T1-weighted sequences (TR 579 ms, TE 9.9 ms, turbo factor 72, refocusing angle 150°, slice thickness 3 mm, FOV 260 mm^2). Moreover, MR-neurography data

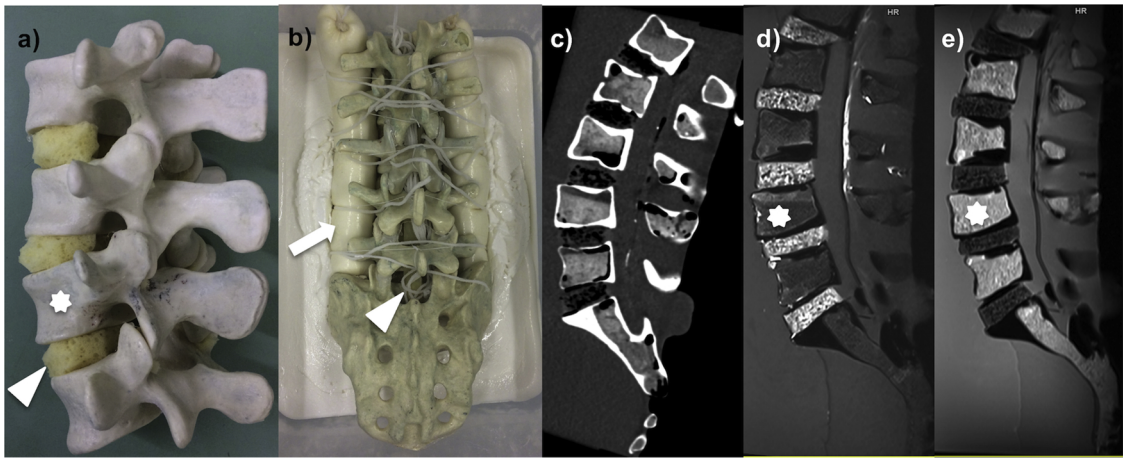

Fig. 4. a) illustrates lumbar vertebrae (star) made of solidified resin from silicon negative casts that were connected by agarose gel fixed polyethylene foam pads in order to imitate intervertebral discs (arrowhead). b) shows the assembled anthropomorphic spine phantom (arrow head: cauda equine; arrow: psoas muscle). For illustration purposes the erector spinae muscles are not shown. c) shows a CT scan of the phantom illustrating the cortical and cancellous bone equivalent densities. d) and e) demonstrate T2- and T1-weighted MRI images of the phantom. The bone marrow appears hypointense in T2 and hyperintense in T1 (star).

were acquired with a 3D "Sampling Perfection with Application optimized Contrasts using different flip angle Evolution" (SPACE) “Short Tau Inversion Recovery” (STIR) sequence resulting in a uniform fat suppression and adequate nerve visualization (TR 2200 ms, TE 135 ms, inversion time 210 ms, flip angle 120°, slice thickness 1 mm, FOV 280 mm^2).

Volumetric FPCT data were acquired on an interventional angiography unit (Artis Zeego, Siemens Healthineers, Erlangen, Germany) using a standard body DynaCT protocol (number of projections 197, angular range 180°, acquisition time 5 s, dose 0.36 µGy/projection, tube peak voltage 95 kV, total mAs 400). Post processing and volume fusion were performed using the respective fusion tool of a syngo X Workplace: VB21 (Siemens Healthineers, Erlangen, Germany).

3. Results

3.1. In vivo MR and CT measurements

Physiologic MR T1 and T2 mapping values of fat, muscle and bone marrow in healthy volunteers yielded reproducible values of 394 ± 16 ms, 1160 ± 45 ms and 822 ± 21 ms for T1 and of 161 ± 10 ms, 40 ± 14 ms and 67 ± 6 for T2 measurements, respectively. Resulting acquisitions are depicted in Fig. 2 in a healthy volunteer.

Mean CT attenuation values for cortical bone corresponded to 1’115 ± 80 HU and 220 ± 15 HU for bone marrow.

3.2. Ex vivo MR and CT measurements

Ex vivo mapping of the castor oil serial dilution resulted in T1 values ranging from 1900 ms to 160 ms and in T2 values ranging from 160 to 20 ms (Table 1), respectively as depicted in Fig. 3a and b (right hand side).

A castor oil concentration of 30% mixed with agarose, purified water and polysorbate 80 revealed approximately identical T1 and T2 relaxation times compared to muscle (ex vivo T1 1040 ± 68 ms, T2 67 ± 2 ms versus in vivo T1 1160 ± 45 ms, T2 40 ± 14 ms). Due to high viscosity and stability of the lipogels, a castor oil concentration of 50% imitated best fat tissue signal (ex vivo T1 575 ± 69 ms, T2 38 ± 2 ms versus in vivo T1 394 ± 16 ms, T2 67 ± 6 ms). Bone marrow signal was reproduced best with a castor oil concentration of 40% (ex vivo T1 755 ± 38 ms, T2 47 ± 1 ms versus in vivo T1 822 ± 21 ms, T2 67 ± 6 ms).

Table 1
Ex vivo mapping of T1 and T2 relaxation times of ten different falcon tubes containing the optimized agarose, purified water, Polyoxyethylen (20)-sorbitan-monooleate gels enriched with varying castor oil concentrations (mass %). Mean values resulted from 6 measurements.

Tube No.	Castor oil %	t1 [ms] ± SD	t2 [ms] ± SD
1	0	1899 ± 70	162 ± 5
2	0	1887 ± 93	162 ± 7
3	5	1740 ± 77	135 ± 8
4	10	1638 ± 47	113 ± 4
5	20	1369 ± 27	79 ± 1
6	30	1040 ± 68	67 ± 2
7	40	755 ± 38	47 ± 1
8	50	575 ± 69	38 ± 2
9	70	287 ± 115	28 ± 1
10	100	156 ± 22	18 ± 1

In order to mimic CT bone density of the anthropomorphic model serial dilution of $CaCO_3$ and $BaSO_4$ in synthetic resin was performed. The testing of different concentrations proved that a $CaCO_3$ concentration of 30% presents ideal viscosity values for the phantom molding during the construction process. However, the maximum achievable density with 30% $CaCO_3$ reached only 636 ± 22 HU. Therefore, $BaSO_4$ was added as a highly x-ray attenuating agent. With a mixture consisting of 30% $CaCO_3$ and 1.5% $BaSO_4$ adequate x-ray attenuation was achieved (ex vivo 1205 ± 179 HU versus in vivo 1’115 ± 80 HU), imitating ideally cortical bone. Consequently, to produce 100 g of cortical bone imitating gel, 68.5 g of synthetic polyurethane resin, 30 g of $CaCO_3$ and 1.5 g of $BaSO_4$ was used. For cancellous bone 10% $CaCO_3$ (10 g for 100 g gel) without $BaSO_4$ in resin (90 g for 100 g gel) was used (ex vivo 190 ± 9 HU versus in vivo 220 ± 15 HU). Table 2 and Fig. 3c illustrate the radio opacity measurements of varying $CaCO_3$ and $BaSO_4$ mixtures in resin.

3.3. Phantom building

The anthropomorphic phantom was eventually successfully assembled. Embedded in lipogel, imitating fat tissue, the phantom was robust, transportable and according to the chief interventionalist of our department haptically comparable to in vivo conditions during needle insertion and advancement (Fig. 4b).

In order to verify anthropomorphic properties of the phantom we

Table 2
CT radio opacity measurements: Ex vivo radio opacity measurements (HU) in 15 tubes filled with a composition of polyurethane resin and different $CaCO_3$ / $BaSO_4$ concentrations.

Tube No.	$CaCO_3$ %	$BaSO_4$ %	HU ± SD
1	0	0	−20 ± 9
2	5	0	58 ± 10
3	10	0	190 ± 9
4	20	0	406 ± 12
5	30	0	636 ± 22
6	40	0	906 ± 33
7	30	0.50	791 ± 394
8	30	0.75	551 ± 67
9	30	1.00	641 ± 62
10	30	1.25	761 ± 97
11	30	1.50	1205 ± 179
12	30	1.75	1466 ± 144
13	30	2.00	2203 ± 134
14	40	1.50	3000 ± 137
15	40	2.00	3015 ± 77

Note: With 30% CaCO3 an optimal moulding property of the bone material is achieved to build a hollow vertebra body. Therefore, BaSO4 was added to reach bone like attenuations.
HU: Hounsfield unit ; $CaCO_3$: calcium carbonate; $BaSO_4$: barium sulphate.

performed clinical used T1-weighted and T2-weighted MR pulse sequences, using the scan protocol mentioned above, and a CT scan proving as well its anthropomorphic properties (see Fig. 4c–e). Comparing the in vivo data of volunteers and the ex vivo data, the final anthropomorphic phantom yielded comparable results in T1 and T2 mapping as well as HU measurements of bony tissue in CT.

3.4. MR neurography and FPCT fusion

A 3D SPACE STIR MR sequence for MRN depicted the cauda equina and nerve roots as shown in Fig. 5c. This isovolumetric MR data set was subsequently fused, using a syngo X Workplace: VB21 (Siemens Healthineers, Erlangen, Germany), with the acquired FPCT in the angio suite. Fig. 5c demonstrates the final, successful fusion of the MRN with the FPCT, depicting the anatomy of the cauda equina and lumbar nerve roots exiting the spinal canal and neuroforamina enclosed by the lumbar vertebra. Fig. 5d–f show a simulated percutaneous nerve root infiltration using syngo iGuide software for needle guidance and trajectory planning resulting in accurate needle placement owing to the additional MRN image information.

4. Discussion

The present feasibility study demonstrates the successful assembly of an anthropomorphic spine phantom, resulting in CT and MRI contrasts equivalent to a human body. Furthermore, nerve tissue was successfully simulated, using agarose impregnated polyethylene fibers. In a last step we were able to fuse MRN with interventional FPCT, combining high-contrast nerve with high-resolution bone tissue and thereby facilitating optimal image guided spine intervention.

A major complication in spinal interventions, such as vertebral/

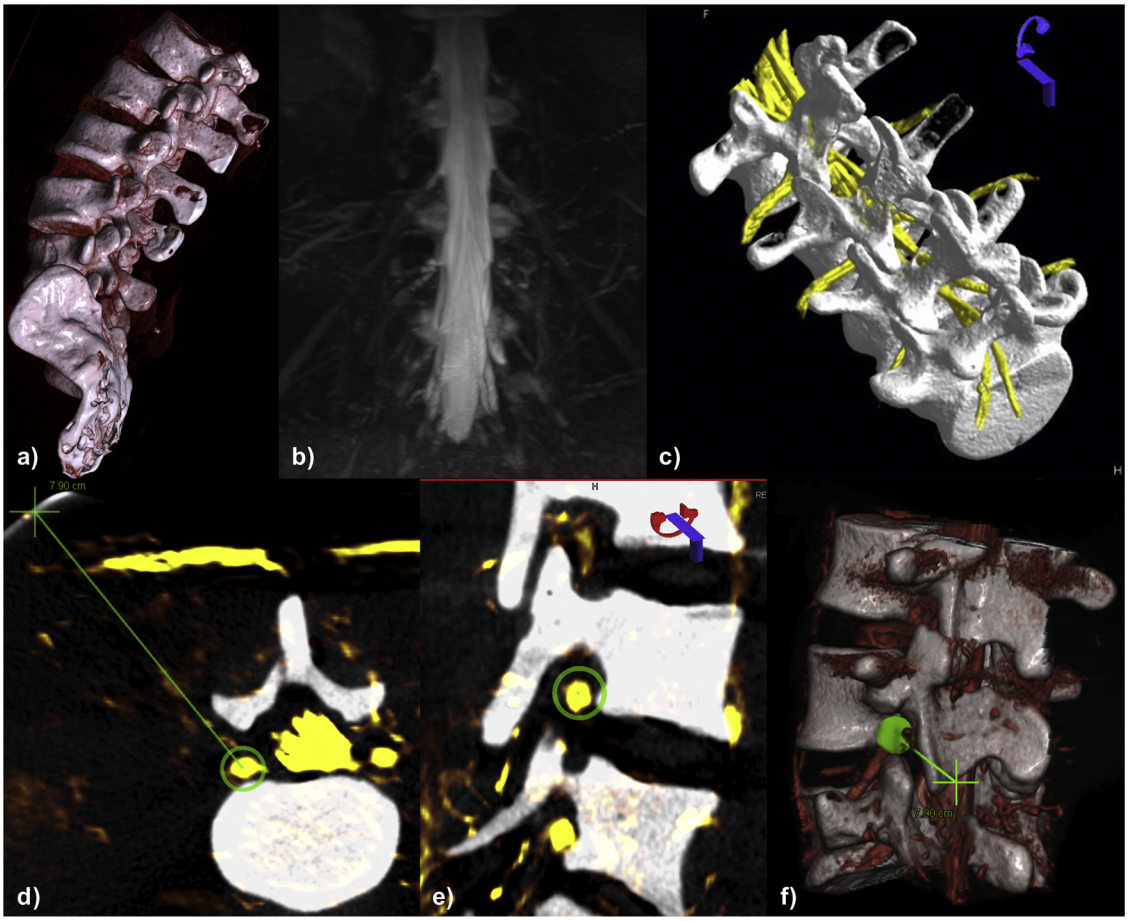

Fig. 5. Final fusion experiment of the FPCT and MRN of the assembled anthropomorphic phantom. Figure a) shows 3D volume rendered reconstruction of an FPCT of the phantom. MIP view of the MRN of the phantom is shown in b). Ultimately c) demonstrates the fusion of the FPCT and MRN, nicely depicting the cauda equina and nerve roots (yellow) exiting the neural foramina on both sides. In d) to f) fusion-based nerve root targeting with syngo iGuide is demonstrated during the simulated intervention with a bulls-eye- and perpendicular-view of needle trajectory (5d and 5e) and additional VRT-Fusion (5f).

intervertebral disc biopsy, vertebroplasty, percutaneous local ablative procedures and nerve root infiltration, is nerve damage or irritation as they cannot be depicted in FPCT or under fluoroscopy. One possibility to overcome this issue is depicting nerve anatomy by image fusion. Fusion of MRN and FPCT enables the interventional radiologist to visualize, in this case the nerve structures during fluoroscopically or CT-guided intervention resulting in safer procedures. In addition, the introduced anthropomorphic phantom may allow preparing and conducting different interventions step by step without limitations in radiation exposure, time restrictions or patient movement, but still under real life conditions in the angiography suite.

Different studies have concentrated on MRI phantoms and even fusion of CT and MRI tissue properties in a single phantom [14–16]. Moreover, several manufacturers offer complete spine models, which have CT equivalent densities and allow CT imaging. To our knowledge there is only one manufacturer (Computerized Imaging Reference Systems, Incorporated, VA, USA) selling a lumbar phantom with tissue properties allowing MRI and CT imaging, however without the ability of depicting nerve structures by MRN. Demonstrating an anthropomorphic phantom allowing for the latter is novel and allows image fusion with structures not visible under mere fluoroscopy or FPCT.

In order to achieve this, first in vivo measurements were performed to retrieve T1 and T2 baseline relaxation times in order to establish a tissue-mimicking phantom. The established in vivo T1 and T2 relaxation times are consistent with published data by de Bazelaire et al for muscle (T1 1160 ± 45 ms, T2 40 ± 14 ms; reported T1 898 ± 33 ms; T2 29 ± 4 ms), bone marrow (T1 822 ± 21 ms, T2 67 ± 6 ms; reported T1 586 ± 73 ms, T2 49 ± 4 ms) and fat tissue (T1 394 ± 16 ms, T2 161 ± 16 ms; reported T1 382 ± 13 ms, T2 68 ± 4 ms) [17]. These tissue relaxation times were successfully simulated by a mixture of agarose, purified water, polysorbate 80 and different concentrations of castor oil. Additionally, CT density was mimicked by adding a mixture of $CaCO_3$ and $BaSO_4$ to resin, resulting in an anthropomorphic, transportable phantom, haptically comparable to in vivo conditions.

The 3D SPACE STIR as used in this study for MRN is also the main sequence in various clinical protocols for examinations of the brachial, lumbar plexus or peripheral nerve pathology [9,18]. Since its first description in 1992 by Howe et al [19], MRN has experienced a steep increase in popularity in diagnostic radiology for depiction of nerve anatomy and pathology [9], mainly due to progress in clear, high resolution depiction of nerve fibers and structures, e.g. plexus at large imaging field of views with homogenous fat saturation [11]. From an interventional perspective, this offers the opportunity of integrating information on nerve anatomy and condition from MRN into large intraprocedural FPCT volumes, allowing the interventionalist to respect, avoid or specifically aim at these structures in different body regions.

There are several limitations to this study. First, it is a phantom study focusing on simulating imaging appearance of different human tissues in both CT and MR. Although comparable to in vivo conditions, the haptic properties were not the main focus of this study but may of course impact on the successful simulation of interventions. Second, nerves in the spinal canal of the phantom were not surrounded by water, i.e. cerebrospinal liquor as this would have further complicated the fabrication process. Last, as the design and production process of the phantom assembly is quite demanding and time consuming, scaling-up towards a reproducible production process should be addressed. 3D printing becomes widely available and incorporated into clinical routine, especially in surgery and intervention planning [20]. Based on our experience from this work we aim to design a 3D printable lumbar spine phantom for large scale fabrication, possessing MRI and CT imaging properties for image fusion.

In conclusion, this study presents a novel anthropomorphic spine model allowing for MRN nerve depiction and image fusion with FPCT in an angiography suite. The customized phantom showed analogous tissue contrasts to in vivo conditions in both MRN and FPCT, facilitating simulations of fusion-image guided spine interventions.

Funding

This research did not receive any specific grant from funding agencies in the public, commercial, or not-for-profit sectors.

Ethical approval

All procedures performed in studies involving human participants were in accordance with the ethical standards of the institutional and/or national research committee and with the 1964 Helsinki declaration and its later amendments or comparable ethical standards.

Informed consent

Informed consent was obtained from all individual participants included in the study.

Conflict of interest

The authors declare that they have no conflict of interest.

References

[1] K.J.M. Surry, H.J.B. Austin, A. Fenster, T.M. Peters, Poly(vinyl alcohol) cryogel phantoms for use in ultrasound and MR imaging, Phys. Med. Biol. 49 (2004) 5529–5546.
[2] S. Ohno, H. Kato, T. Harimoto, Y. Ikemoto, K. Yoshitomi, S. Kadohisa, et al., Production of a human-tissue-equivalent MRI phantom: optimization of material heating, Magn. Reson. Med. Sci. 7 (2008) 131–140.
[3] L. Appelbaum, S.Y. Mahgerefteh, J. Sosna, S.N. Goldberg, Image-guided fusion and navigation: applications in tumor ablation, Tech. Vasc. Interv. Radiol. 16 (2013) 287–295, https://doi.org/10.1053/j.tvir.2013.08.011.
[4] M. Rajagopal, A.M. Venkatesan, Image fusion and navigation platforms for percutaneous image-guided interventions, Abdom. Radiol. (NY). 41 (2016) 620–628, https://doi.org/10.1007/s00261-016-0645-7.
[5] N. Abi-Jaoudeh, J. Kruecker, S. Kadoury, H. Kobeiter, A.M. Venkatesan, E. Levy, et al., Multimodality image fusion-guided procedures: technique, accuracy, and applications, Cardiovasc. Intervent. Radiol. 35 (2012) 986–998, https://doi.org/10.1007/s00270-012-0446-5.
[6] G. Tsoumakidou, C.W. Too, G. Koch, J. Caudrelier, R.L. Cazzato, J. Garnon, et al., CIRSE guidelines on percutaneous vertebral augmentation, Cardiovasc. Intervent. Radiol. 40 (2017) 331–342, https://doi.org/10.1007/s00270-017-1574-8.
[7] L. Manchikanti, S. Abdi, S. Atluri, R.M. Benyamin, M.V. Boswell, R.M. Buenaventura, et al., An update of comprehensive evidence-based guidelines for interventional techniques in chronic spinal pain. Part II: guidance and recommendations, Pain Physician. 16 (2013) S49–283.
[8] T. Soldatos, G. Andreisek, G.K. Thawait, R. Guggenberger, E.H. Williams, J.A. Carrino, et al., High-resolution 3-T MR neurography of the lumbosacral plexus, Radiographics 33 (2013) 967–987, https://doi.org/10.1148/rg.334115761.
[9] A. Chhabra, A.J. Madhuranthakam, G. Andreisek, Magnetic resonance neurography: current perspectives and literature review, Eur. Radiol. 28 (2017), https://doi.org/10.1007/s00330-017-4976-8 328–10.
[10] R. Guggenberger, D. Markovic, P. Eppenberger, A. Chhabra, A. Schiller, D. Nanz, et al., Assessment of median nerve with MR neurography by using diffusion-tensor imaging: normative and pathologic diffusion values, Radiology 265 (2012) 194–203, https://doi.org/10.1148/radiol.12111403.
[11] X. Wang, C. Harrison, Y.K. Mariappan, K. Gopalakrishnan, A. Chhabra, R.E. Lenkinski, et al., MR Neurography of brachial plexus at 3.0 T with robust fat and blood suppression, Radiology 283 (2017) 538–546, https://doi.org/10.1148/radiol.2016152842.
[12] H. Kato, M. Kuroda, K. Yoshimura, A. Yoshida, K. Hanamoto, S. Kawasaki, et al., Composition of MRI phantom equivalent to human tissues, Med. Phys. 32 (2005) 3199–3208, https://doi.org/10.1118/1.2047807.
[13] K. Yoshimura, H. Kato, M. Kuroda, A. Yoshida, K. Hanamoto, A. Tanaka, et al., Development of a tissue-equivalent MRI phantom using carrageenan gel, Magn. Reson. Med. 50 (2003) 1011–1017, https://doi.org/10.1002/mrm.10619.
[14] D. Mitsouras, T.C. Lee, P. Liacouras, C.N. Ionita, T. Pietilla, S.E. Maier, et al., Three-dimensional printing of MRI-visible phantoms and MR image-guided therapy

simulation, Magn. Reson. Med. 77 (2017) 613–622, https://doi.org/10.1002/mrm.26136.
[15] A. Hellerbach, V. Schuster, A. Jansen, J. Sommer, MRI phantoms - are there alternatives to agar? PLoS One 8 (2013) e70343, , https://doi.org/10.1371/journal.pone.0070343.
[16] R.R. Gallas, N. Hünemohr, A. Runz, N.I. Niebuhr, O. Jäkel, S. Greilich, An anthropomorphic multimodality (CT/MRI) head phantom prototype for end-to-end tests in ion radiotherapy, Z. Med. Phys. 25 (2015) 391–399, https://doi.org/10.1016/j.zemedi.2015.05.003.
[17] C.M.J. de Bazelaire, G.D. Duhamel, N.M. Rofsky, D.C. Alsop, MR imaging relaxation times of abdominal and pelvic tissues measured in vivo at 3.0 T: preliminary results, Radiology 230 (2004) 652–659, https://doi.org/10.1148/radiol.2303021331.
[18] A. Chhabra, J. Carrino, Current MR neurography techniques and whole-body MR neurography, Semin. Musculoskelet. Radiol. 19 (2015) 79–85, https://doi.org/10.1055/s-0035-1545074.
[19] F.A. Howe, A.G. Filler, B.A. Bell, J.R. Griffiths, Magnetic resonance neurography, Magn. Reson. Med. 28 (1992) 328–338.
[20] D. Mitsouras, P. Liacouras, A. Imanzadeh, A.A. Giannopoulos, T. Cai, K.K. Kumamaru, et al., Medical 3D printing for the radiologist, Radiographics 35 (2015) 1965–1988, https://doi.org/10.1148/rg.2015140320.